

Iterative Decomposition of Water and Fat With Echo Asymmetry and Least-Squares Estimation (IDEAL): Application With Fast Spin-Echo Imaging

Scott B. Reeder,^{1*} Angel R. Pineda,¹ Zhifei Wen,¹ Ann Shimakawa,² Huanzhou Yu,¹ Jean H. Brittain,² Garry E. Gold,¹ Christopher H. Beaulieu,¹ and Norbert J. Pelc¹

Chemical shift based methods are often used to achieve uniform water-fat separation that is insensitive to B_0 inhomogeneities. Many spin-echo (SE) or fast SE (FSE) approaches acquire three echoes shifted symmetrically about the SE, creating time-dependent phase shifts caused by water-fat chemical shift. This work demonstrates that symmetrically acquired echoes cause artifacts that degrade image quality. According to theory, the noise performance of any water-fat separation method is dependent on the proportion of water and fat within a voxel, and the position of echoes relative to the SE. To address this problem, we propose a method termed “iterative decomposition of water and fat with echo asymmetric and least-squares estimation” (IDEAL). This technique combines asymmetrically acquired echoes with an iterative least-squares decomposition algorithm to maximize noise performance. Theoretical calculations predict that the optimal echo combination occurs when the relative phase of the echoes is separated by $2\pi/3$, with the middle echo centered at $\pi/2 + \pi k$ ($k = \text{any integer}$), i.e., $(-\pi/6 + \pi k, \pi/2 + \pi k, 7\pi/6 + \pi k)$. Only with these echo combinations can noise performance reach the maximum possible and be independent of the proportion of water and fat. Close agreement between theoretical and experimental results obtained from an oil-water phantom was observed, demonstrating that the iterative least-squares decomposition method is an efficient estimator. Magn Reson Med 54:636–644, 2005. © 2005 Wiley-Liss, Inc.

Key words: fat suppression; fast spin echo; magnetic resonance imaging; water-fat separation; asymmetric echoes; brachial plexus

Reliable and uniform fat suppression is essential for accurate diagnoses in many areas of MRI. This is particularly true for sequences such as fast spin-echo (FSE) imaging, in which fat is bright and may obscure underlying pathology. Although conventional fat saturation may be adequate for areas of the body with a relatively homogeneous B_0 field, there are many applications in which fat saturation routinely fails. This is particularly true for extremity imaging, off-isocenter imaging, large field of view (FOV) imaging, and challenging areas such as the brachial plexus and

skull base, as well as many others. Short-TI inversion recovery (STIR) imaging provides uniform fat suppression, but at a cost of a reduced signal-to-noise ratio (SNR) and mixed contrast that is dependent on T_1 (1). This latter disadvantage limits STIR imaging to T_2 -weighted (T_2W) applications, and current T_1 -weighted (T_1W) applications rely solely on conventional fat-saturation methods. Another fat-suppression technique used with FSE is the application of spectral-spatial pulses; however, this method is also sensitive to field inhomogeneities (2,3).

“In and out of phase” imaging was first described by Dixon (4) in 1984, and was used to exploit the difference in chemical shifts between water and fat in order to separate water and fat into separate images. Glover (5) and Glover and Schneider (6) further refined this approach in 1991 with a three-point method that accounts for B_0 field inhomogeneities. Hardy et al. (7) first applied this method to FSE imaging by acquiring three images with the readout centered at the SE for one image, and symmetrically before and after the SE in the subsequent two images. These water-fat separation methods have since been combined with both SE and FSE imaging for many applications (8–13). Several of these three-point approaches acquire one image with the readout centered at the SE and the other two acquired symmetrically on each side of the SE (5,7,13). This approach has the advantage of minimizing the time between refocusing pulses of the FSE train while providing sufficient time between echoes for phase between water and fat to evolve. Initial descriptions of the relationship between the echo spacing and the noise performance of the water-fat decomposition have been reported (5,8,13); however, these approaches do not fully characterize the theoretical noise performance of water-fat separation methods.

It was recently demonstrated that decomposition of water from fat with symmetrically acquired echoes cannot be achieved when the proportions of water and fat within a voxel are approximately equal (14–16). A complete characterization of the theoretical maximum noise performance of water-fat decomposition, including the effects of field inhomogeneity estimation, was reported by Pineda et al. (15,16). This work showed that the theoretical ability of all water-fat separation methods to decompose water from fat in a voxel is dependent on the relative proportions of water and fat, as well as the position of acquired echoes relative to the SE. The dependence on the proportions of water and fat is particularly true for echoes that are acquired symmetrically about the SE.

In this work we show both qualitatively and quantitatively a strong dependence of the noise performance of

¹Department of Radiology, Stanford University Medical Center, Stanford, California, USA.

²Applied Science Lab-West, GE Healthcare, Menlo Park, California, USA.

Grant sponsor: NIH; Grant numbers: P41 RR09784; 1RO1-EB002524; Grant sponsors: Lucas Foundation; GE Healthcare.

*Correspondence to: Scott B. Reeder, M.D., Ph.D., Department of Radiology, E3/311 CSC, 600 Highland Avenue, Madison, WI, 53792. E-mail: sreeder@wisc.edu.

Received 28 July 2004; revised 11 April 2005; accepted 18 April 2005.

DOI 10.1002/mrm.20624

Published online 9 August 2005 in Wiley InterScience (www.interscience.wiley.com).

© 2005 Wiley-Liss, Inc.

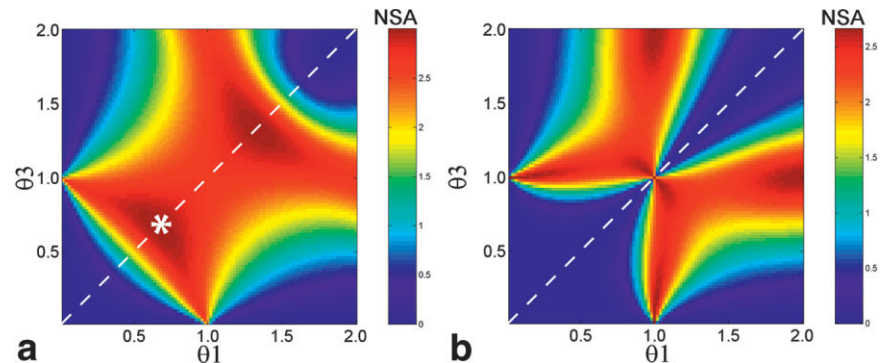


FIG. 1. Theoretical NSA calculated against θ_1 and θ_3 for a voxel with (a) all water and (b) water \approx fat, when θ_2 is fixed at zero at the SE. Symmetrically acquired echoes occur along the dashed line. Phase is plotted in units of π . The asterisk indicates the optimal spacing ($2\pi/3$) for the case in which the voxel contains all water.

water–fat decomposition using echoes acquired symmetrically about an SE on the fat : water ratio within a voxel and the choice of echo position. We propose a method termed “iterative decomposition of water and fat with echo asymmetric and least-squares estimation” (IDEAL). This technique combines the acquisition of echoes acquired asymmetrically with respect to the SE, and a recently described iterative least-squares water–fat separation decomposition algorithm in order to maximize the noise performance of the water–fat decomposition. The behavior of symmetric and asymmetric echoes is verified with an oil–water phantom using an iterative least-squares water–fat decomposition method that permits the use of arbitrary and unequally spaced echoes (13). Examples obtained in volunteers and patients are shown for various applications, including T_2W and T_1W imaging.

THEORY

The phase shift between water and fat as a result of chemical shift is

$$\theta = 2\pi \Delta f t \quad [1]$$

where Δf is the chemical shift (Hz) between water and fat, and t is the time relative to the SE. It is preferable to calculate echo shifts in terms of θ , rather than t , because θ is independent of field strength and provides more physical intuition.

The noise performance of a water–fat decomposition is conveniently described with the effective number of signal averages (NSA), which can be defined as

$$NSA = \frac{\sigma^2}{\sigma_p^2} \quad [2]$$

where σ^2 is the variance of the noise in a source image and σ_p^2 is the variance of the noise in a calculated water or fat image. Equation [2] is a helpful measure of the noise performance of a water–fat decomposition. For any three-point water–fat decomposition method, the maximum possible NSA is 3, which is equivalent to what would be obtained if the object contained only water or only fat, and the three source images were averaged (5).

Figure 1a shows a 2D plot of the theoretical maximum NSA of a calculated water image from three source images acquired with echoes θ_1 and θ_3 shifted with respect to the SE, when θ_2 is held fixed at zero and the voxel contains mostly water (15,16). For symmetrically acquired echoes (dashed line), the NSA increases to a maximum of 3 when $\theta_1 = -2\pi/3$ and $\theta_3 = 2\pi/3$ (asterisk, Fig. 1a). This combination of echoes ($-2\pi/3, 0, 2\pi/3$) is the optimum choice for this case, and is an intuitive result that reflects equal sampling around the unit circle (6). Figure 1b plots the theoretical NSA for equal proportions of water and fat. From this plot it can be seen that NSA is zero for almost all choices of θ_1 and θ_3 , reflecting the fact that no water–fat decomposition method can resolve water from fat when they are in equal proportions. The only echo combination that produces a nonzero NSA is $(-\pi, 0, \pi)$. However, this is a singular result and any small deviation from this echo spacing (e.g., $-0.99\pi, 0, 0.99\pi$) results in $NSA \sim 0$ at this fat : water ratio. The overall behavior of Fig. 2 agrees with the geometrical prediction made by Wen et al. (14).

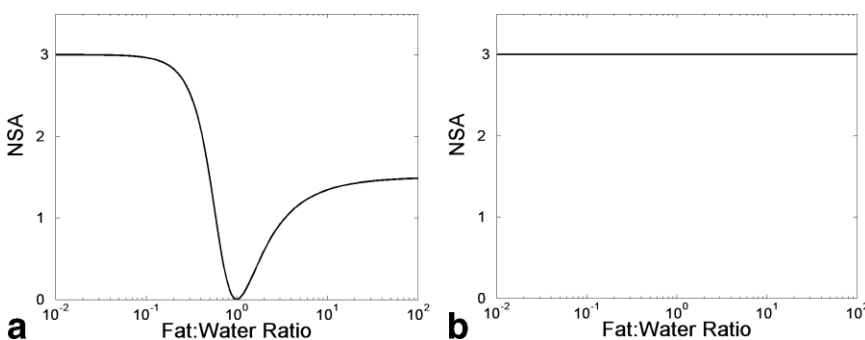


FIG. 2. Theoretical maximum NSA of pixels in a calculated water image as a function of fat : water ratio for (a) symmetric echoes ($-2\pi/3, 0, 2\pi/3$; black curve), and (b) asymmetric echoes ($-\pi/6, \pi/2, 7\pi/6$).

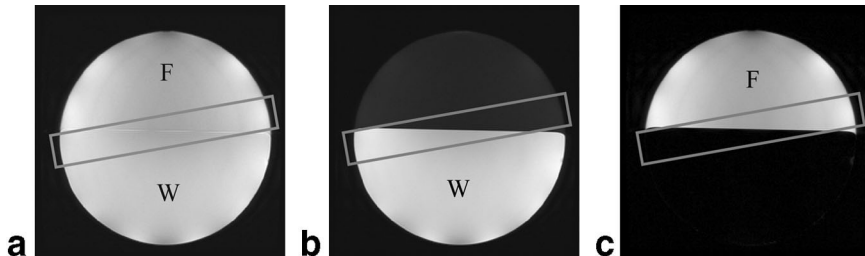


FIG. 3. Axial IDEAL FSE images through the oil–water phantom at 1.5T, schematically illustrating the obliquely prescribed slice (a) recombined image, (b) calculated water image, and (c) calculated fat image. This slice creates a continuum of fat:water ratios across the slice through partial-volume effects. Note that there is a small amount of water signal with the oil region (b). W = water, F = fat.

This effect is better illustrated in Fig. 2a, which plots the theoretical maximum NSA of a calculated water image against the fat : water ratio for symmetrically spaced echoes ($-2\pi/3, 0, 2\pi/3$). From this figure it can be seen that NSA meets the theoretical maximum (3) when the voxel contains mostly water, and there is a broad minimum when water and fat are in similar proportions. It is also interesting to note that the theoretical NSA recovers to only ~ 1.4 when the voxel contains mostly fat.

We calculated the NSA over a wide range of echo shifts ($\theta_1, \theta_2, \theta_3$) and fat:water ratios to determine the combination that maximized noise performance. From this analysis we found that the combination of three echoes that maximized the NSA were those separated by $2\pi/3$, with the middle echo centered at $\pi/2 + \pi k$ (k = any integer), i.e., $(-\pi/6 + \pi k, \pi/2 + \pi k, 7\pi/6 + \pi k)$. For practical SE and FSE applications, the optimum echo combinations that minimize the time between refocusing pulses are $(-\pi/6, \pi/2, 7\pi/6)$ and $(-\pi/6, -\pi/2, \pi/6)$, which are equivalent from the perspective of refocusing pulse spacing. Figure 2b plots the theoretical maximum NSA against the fat:water ratio for asymmetric echoes (IDEAL). A tremendous improvement in NSA from asymmetric echoes is seen in comparison with the symmetric echoes, since the NSA reaches the upper limit of 3 and is independent of the fat : water ratio within a voxel.

MATERIALS AND METHODS

Phantom experiments were performed to quantitatively validate the theoretical noise behavior of the water–fat decomposition. A spherical phantom consisting of peanut oil floating on 0.9% normal saline doped with 5 mM NiCl₂ was imaged at 1.5T with an FSE pulse sequence modified to shift the readout gradient with respect to the SEs (13). Figure 3 shows axial calculated water (b) and fat (c) images, as well as a recombined (a) image through the oil–water phantom. From this plane an obliquely oriented slice was prescribed through the oil–water interface to create a continuum of fat:water ratios. An extremity coil and the following image parameters were used: $N_x = 256$, $N_y = 256$, averages = 1, FOV = 20 cm, slice = 9 mm, echo train length (ETL) = 16, BW = ± 31.3 kHz, and TR/TE = 700/13.1 ms. TR and TE were empirically chosen to produce similar signal intensities from both water and fat. Various combinations of symmetric and asymmetric echoes were used. Although the time between refocusing pulses (echo spacing) will vary with different echo shifts, it was fixed at 13.1 ms to ensure that the MR signals, as well as potential blurring in the phase-encoding direction,

were identical for all cases. Product automated shim routines were used for all of the phantom imaging.

For each combination of echoes, the phantom image acquisition was repeated 200 times (scan time = 2 hr 5 min, for 200 acquisitions), and water and fat images were reconstructed with an online algorithm based on an iterative least-squares algorithm, which easily accommodates arbitrary TEs (13). This algorithm uses a “robust” region-growing reconstruction algorithm (17) to prevent the water–fat ambiguities that are commonly seen with water–fat decomposition algorithms (5,6,17). The region-growing algorithm uses field map estimates from nearby pixels to improve the initial guess of the field map, ensuring that the iterative algorithm converges to the correct solutions for the field map, water, and fat. Although field map information from nearby pixels is used, it does not affect the noise performance of the water–fat decomposition for a given pixel. The reason for this is analogous to phase-unwrapping algorithms used with other water–fat separation methods, that use a binary algorithm to choose between two possible solutions, leaving the noise performance of the solutions themselves unaffected (8,18,19). Smoothing of the field map estimate, followed by computation of fat and water signals based on the locally smoothed field map, can improve the SNR water–fat decomposition, and may be useful. However, this can also introduce bias or deterministic errors in regions where the actual field map may not be smooth. The effect of field map smoothing on noise performance is an additional complexity that is beyond the scope of this work. The NSA was calculated on an individual pixel basis as the quotient of the variance of each pixel from the three source images and the variance of the calculated water image (Eq. [2]). Pixels outside the phantom were excluded using a threshold mask. For each pixel, the fat:water ratio was calculated from the ratio of the average fat signal (computed over all 200 images) divided by the average water signal (computed over all 200 sets of three source images). In this way, scatter plots of measured NSA vs. fat:water ratio were made. All NSA calculations (theoretical and experimental) were performed with the use of offline programs written in Matlab 6.0 (Mathworks, Natick, MA, USA).

All human scanning was performed at 1.5T (Signa Twin-Speed; GE Healthcare, Milwaukee, WI, USA) and 3.0T (Signa VH/i; GE Healthcare, Milwaukee, WI, USA). The knees, abdomen, and brachial plexus of healthy volunteers and patients were imaged after approval was obtained from our institutional review board (IRB) and informed consent was given by the subjects. We used a modified FSE pulse sequence to acquire three images with different echo

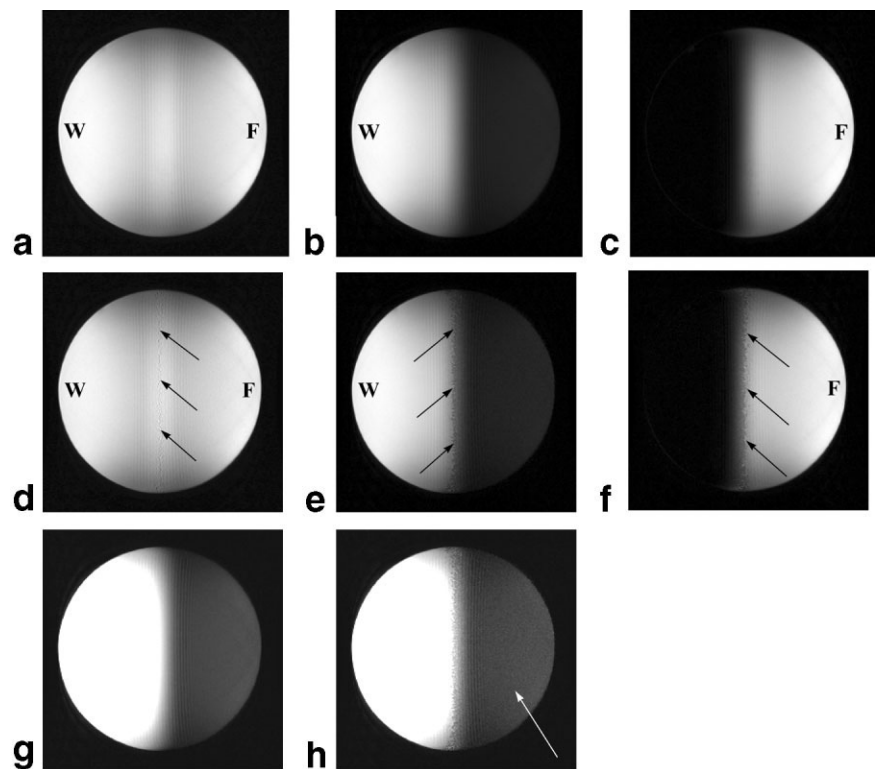


FIG. 4. Oblique FSE images acquired through the oil–water interface of the oil–water phantom with the IDEAL method ($-\pi/6$, $\pi/2$, $7\pi/6$; top row), and symmetric echoes ($-\pi/2$, 0 , $\pi/2$; bottom row). Recombined (a and d), calculated water (b and e), and calculated fat (c and f) images show irregular and noisy signal when water and fat are in similar proportions (black arrows). g and h: The same water images as in b and e, but windowed to better demonstrate the increased noise in the water image from the symmetric acquisition (h) in a region that contains a small amount of water but is mostly fat (white arrow). W = water, F = fat.

shifts. Fat-saturated FSE images were acquired for comparison in many cases. Abdominal and pelvic imaging was performed using a torso phased-array coil, knee imaging was performed with an extremity coil, and brachial plexus imaging was performed with a phased-array neurovascular coil. All water–fat decomposition calculations were performed with an online reconstruction algorithm based on the iterative least-squares algorithm, which is capable of multicoil reconstruction (13).

RESULTS

Figure 4 shows recombined, water, and fat images acquired obliquely through the water–oil interface of the phantom described in Fig. 3, for both asymmetric (IDEAL) (a–c) and symmetric echoes (d–f). The IDEAL water image (g) and symmetric water image (h) are also shown with windowing to better demonstrate the increased noise in the region that is mostly fat signal. The small amount of signal in this region most likely caused olefinic components of the oil that have resonant peaks very close to that of water, reflecting an inherent limitation of all fat-suppression methods that rely on the chemical shift between water and fat (including water–fat decomposition methods) (20). The apparent increase in noise in the symmetric water image can be explained by the curves shown in Fig. 2a for the high fat : water ratio. Note that Fig. 4 also shows very noisy signal in the calculated symmetric water and fat images in which water and fat are in similar proportions (arrows). Drift in the magnitude and phase of these images due to possible system instability was not observed over the acquisition of the 200 images.

Figure 5 plots experimental NSAs from the phantom experiments as a function of the fat : water ratio for four different echo combinations: $(-2\pi/3, 0, 2\pi/3)$, $(-\pi/2, 0, \pi/2)$, $(-\pi/6, \pi/2, 7\pi/6)$, and $(0, \pi/2, \pi)$. Theoretical predictions are shown as solid curves, and very close agreement with experimental measurements is seen. The data from Fig. 5c were fit to the linear equation: $NSA = \text{slope} * \log_{10}(\text{fat:water ratio}) + \text{intercept}$. The intercept and slope were calculated to be 2.901 ± 0.002 , and 0.066 ± 0.001 , respectively, indicating very good agreement between experiment and theory. The apparent scatter of the experimentally measured NSA decreases when NSA approaches zero (Fig. 5a and b). This occurs because NSA is the quotient of the source image variance, which remains constant over all fat : water ratios, and the variance of the calculated water images, which becomes very large when the fat : water ratio approaches one.

The theoretical and experimental plots of NSA performance are shown for the NSA of calculated water images only. A similar analysis was performed for the NSA of the calculated fat images, but for brevity the results are not included here. The theoretical and experimental NSAs of the calculated fat images demonstrate almost identical behavior. The main difference is that the horizontal axis (i.e., the fat : water ratio) is reversed. For example, the NSA of fat for symmetric echoes $(-2\pi/3, 0, 2\pi/3)$ is 3 when the voxel contains all fat instead of all water.

Figure 6 shows calculated water images from a T_2 W sagittal knee acquisition at 3.0T acquired with symmetric echoes (phase shifts = $-2\pi/3$, 0 , $2\pi/3$; time shifts = -0.8 ms, 0 ms, 0.8 ms). For comparison, images acquired with the IDEAL method (phase shifts = $-\pi/6$, $\pi/2$, and

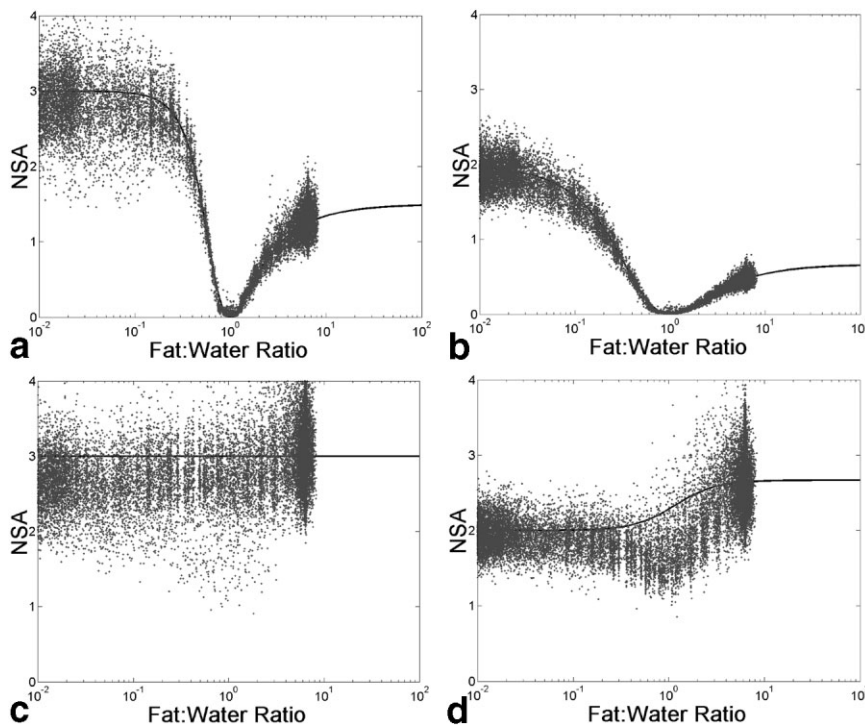


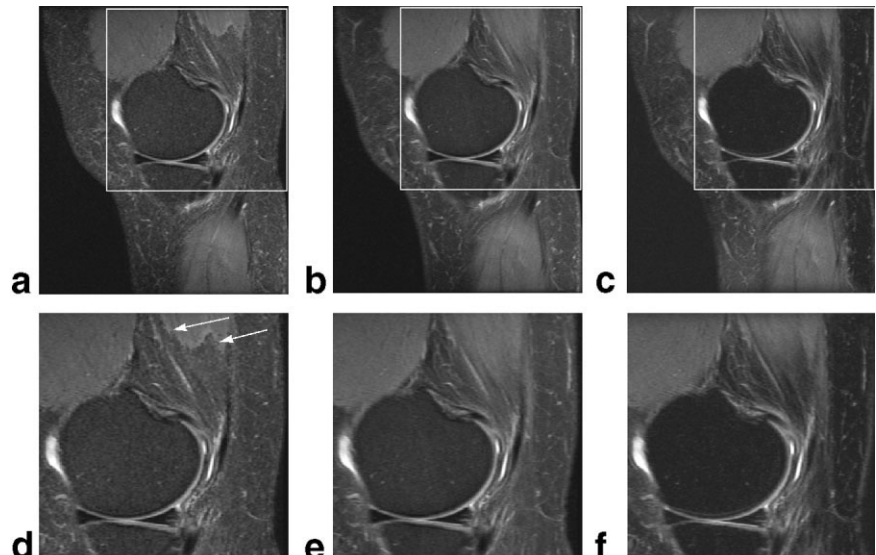
FIG. 5. Experimentally measured NSA (dots) plotted against measured fat : water ratio for **a**) symmetric echoes ($-2\pi/3, 0, 2\pi/3$), **b**) symmetric echoes ($-\pi/2, 0, \pi/2$), **c**) asymmetric echoes ($-\pi/6, \pi/2, 7\pi/6$), and **d**) asymmetric echoes with shortened echo spacing ($0, \pi/2, \pi$). Smooth black lines indicate the theoretical maximum NSA for pixels in the calculated water image. Excellent agreement between experimental measurements and theory is seen.

$7\pi/6$; time shifts = -0.2 ms, 0.6 ms, and 1.4 ms) and conventional fat saturation are also shown, as well as magnified views of all three. Close inspection of these images reveals several artifacts in the symmetric acquisition. Pixels that occur at interfaces between muscle (water signal) and subcutaneous fat are very irregular and non-anatomic. In addition, the signal in the bone marrow and subcutaneous fat appears mottled and noisy. These artifacts are not seen in the IDEAL images and fat-saturated images. Image quality was notably improved for all images acquired with the IDEAL method compared to the symmetric images (not shown).

Several clinical examples acquired with IDEAL imaging are shown in Figs. 7–10. Figure 7 shows recombined,

water, and fat images in the pelvis of a female patient with a right adnexal mass, obtained at 1.5T. Direct visualization of fat within this mass in the calculated fat image is diagnostic of a mature ovarian teratoma (dermoid). Figure 8 shows T_2 W FSE recombined, and calculated water and fat images of the knee of a patient with pre-patellar edema. A comparison with fat-saturated T_2 W images shows an area of failed fat saturation that would lead to erroneous overestimation of the extent of the edema. Figure 9 shows examples of sagittal T_1 W and coronal T_2 W images of the brachial plexus and cervical spine acquired at 1.5T using a neurovascular coil. A comparison with fat-saturated images shows marked improvement in the uniformity of fat suppression across the images. Figure 10 shows two con-

FIG. 6. Sagittal T_2 W FSE images through the knee of a normal volunteer at 3.0T using **(a)** symmetric echoes ($-2\pi/3, 0, 2\pi/3$), **(b)** asymmetric echoes ($-\pi/6, \pi/2, 7\pi/6$) (IDEAL), and **(c)** fat saturation. Images in the second row **(d–f)** are closeup views of corresponding images in a–c. Note the irregular margins between muscle and fat in the symmetric echo image (white arrows), as well as increased noise in the bone marrow and subcutaneous fat. Image parameters: TR/TE = 5000/48 ms, matrix = 384×192 , FOV = 16 cm, slice/gap = $3.0 \text{ mm}/0.5 \text{ mm}$, ETL = 10, BW = ± 31.25 kHz, total scan time for entire knee = 5 min 5 s.



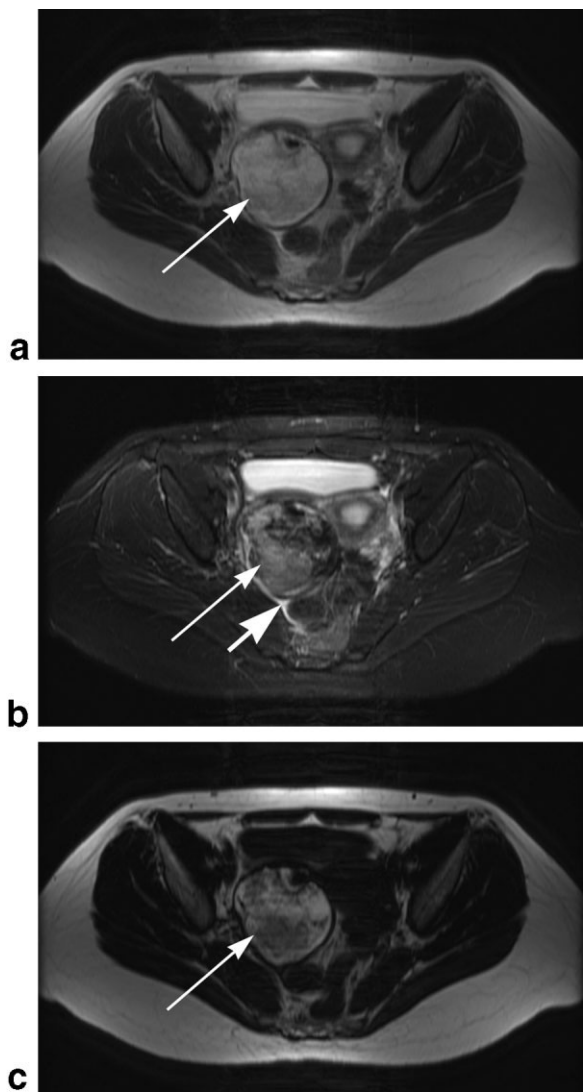


FIG. 7. IDEAL recombined (a), calculated water (b), and calculated fat (c) images through the pelvis of a woman with a mature ovarian teratoma (long arrows) acquired using a torso phased-array coil at 1.5T. The fat image clearly shows the extensive fat content of this mass, and the water image shows subtle amounts of free fluid (short arrow). Image parameters: TR/TE = 5000/60 ms, matrix = 384 × 192, FOV = 40 cm, slice/gap = 9 mm/5 mm, ETL = 10, BW = ±31.25 kHz, total scan time for pelvis = 5 min 5 s.

secutive calculated water images from a T_1 W MR arthrogram, acquired at 1.5T with a torso phased-array coil after intra-articular injection of dilute Gd-DTPA.

DISCUSSION

Echoes acquired symmetrically about an SE can lead to the inability of estimation methods to resolve water from fat when they are in similar proportions within a voxel. This can lead to image artifacts, such as irregular interfaces, and increased noise in certain regions of the image. One can achieve the maximum NSA of 3 for all fat:water ratios by setting the phase of the middle image at $\pi/2 + \pi k$ (k = any integer) and spacing the other two images $2\pi/3$ before and

after the middle image. Theoretical predictions of the maximum NSA were verified experimentally with an oil–water phantom, for several combinations of symmetrical and asymmetrical echoes. The experimental noise performance matched theoretical predictions closely for both symmetric and asymmetric echoes, demonstrating that the iterative method is an efficient estimator that achieves the best possible NSA for a given echo combination (21). With the use of the IDEAL method, the noise performance of water–fat separation in pixels with varying proportions of fat is maximized, the dependence of NSA on the fat:water ratio is eliminated, and the image artifacts that arise with symmetric echo acquisitions are avoided. Several clinical examples acquired with the IDEAL method are shown at both 1.5T and 3.0T, demonstrating the feasibility of both T_1 W and T_2 W imaging to obtain high-quality, high-SNR, multicoil images with uniform water–fat separation.

Three-point water–fat separation methods that position the phase of the center at $\pi/2$ were described by Xiang and An (8), and used by Ma et al. (12) as part of a $(0, \pi/2, \pi)$ combination. Although this choice of echoes helps to reduce the dependence of NSA on the fat:water ratio (Fig. 5d), these implementations were not designed for this purpose. This choice of echoes has the primary advantage of simplifying the analytical solutions that decompose water and fat (8).

Uniform noise performance across all fat:water ratios may be particularly important for special imaging applications that require quantification of the relative amounts of water and fat within tissues (e.g., fatty liver in nonalcoholic steatohepatitis (22), adrenal masses (23), etc.).

One can intuitively understand symmetric echoes, as well as the asymmetric echoes used in the IDEAL method, by realizing that complex images acquired symmetrically before or after an SE are Hermitian conjugates of one another, and therefore contain the same information. In addition, all phase information is lost in echoes that are acquired at the SE when chemical shift and field inhomogeneities are fully refocused. In general, at least three unique images acquired at different TEs are required to resolve water from fat (5,13). If an image is acquired when the phases of water and fat are orthogonal, (i.e., the phase shift between water and fat is $\pi/2 + \pi k$ (k = any integer)), and there are no additional phase shifts from field inhomogeneities or other sources (e.g., coil, receivers, flow, etc.), water and fat could, in theory, be resolved simply from the real and imaginary components of this image, respectively (24,25). However, two additional images are needed to compensate for field inhomogeneities and constant phase shifts. These additional echoes are ideally positioned so that the phase shift from the water–fat chemical shift is sampled equally around the unit circle, i.e., $2\pi/3$ before and after the middle image that is acquired at $\pi/2 + \pi k$.

Water–fat separation methods have several disadvantages. First, the additional time needed to shift readout gradients to acquire echoes at different TEs may reduce sequence efficiency. For FSE, echo shifts will increase the time between refocusing pulses (echo spacing) and lengthen the overall echo train time, and may result in increased blurring (26). This will be most problematic with proton density FSE imaging, in which the central

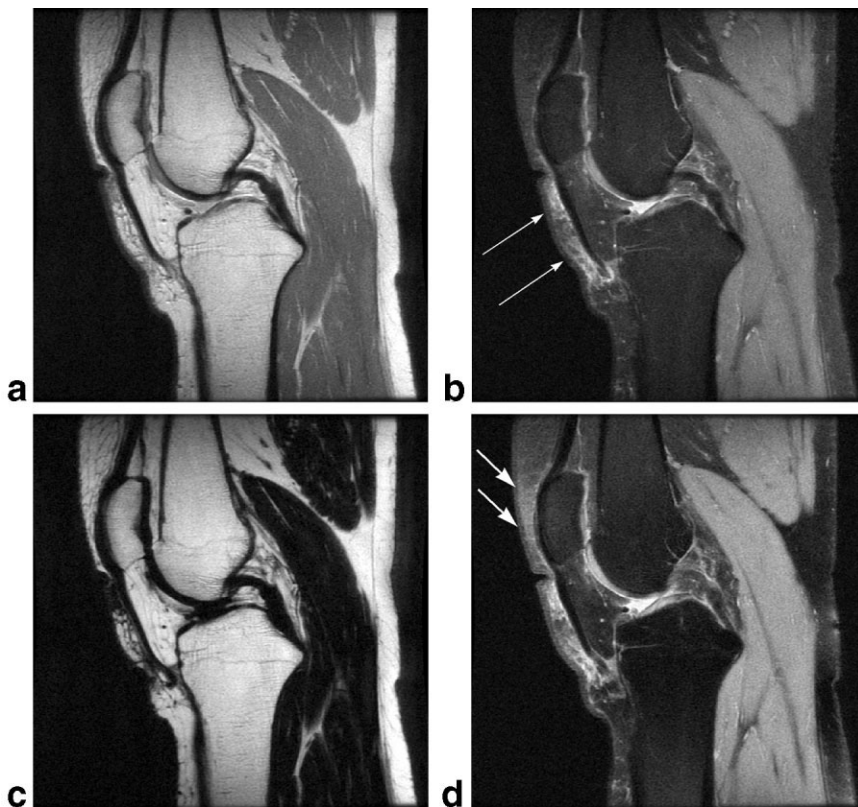


FIG. 8. IDEAL recombined (a), calculated water (b), calculated fat (c) sagittal T₂W FSE images acquired in the knee of a patient volunteer at 1.5T. Pre-patellar edema (long arrows) in the calculated water image is more accurately depicted in the IDEAL water image than in the fat-saturated T₂W image that is shown for comparison (d). Areas of failed fat saturation (short arrow) may have overestimated the extent of the pre-patellar edema. The scan time for the entire knee was 5 min 30 s for both IDEAL and fat saturation methods. Image parameters: TR/TE = 4000/48 ms, matrix = 384 × 256, FOV = 16 cm, slice/gap = 2.5 mm/0.5 mm, ETL = 10, BW = ±31.25 kHz, total scan time for knee = 5 min 20 s.

FIG. 9. Sagittal T₁W IDEAL water (a) and fat-saturated T₁W (b) images of the brachial plexus acquired with a phased-array neurovascular coil. Coronal T₂W IDEAL water (c) and fat-saturated (d) images are also shown. Tremendous improvement in the uniformity of fat suppression is seen in both T₁W and T₂W IDEAL imaging. Note the “pseudo-tumor” appearance of the failed fat saturation just superior to the lung apices (thin arrows) and other regions of failed fat saturation (thick arrows). Image parameters for T₂W images: TR/TE = 4325/55 ms, matrix = 384 × 192, FOV = 24 cm, slice/gap = 4.5 mm/0.5 mm, ETL = 10, BW = ±20 kHz, total scan time for unilateral brachial plexus and cervical spine = 4 min 33 s. Image parameters for T₁W images: TR/TE = 650/12 ms, 384 × 192, FOV = 24 cm, slice/gap = 4.5 mm/0.5 mm, ETL = 2, BW = ±20 kHz, total scan time for unilateral brachial plexus and cervical spine = 6 min 20 s.

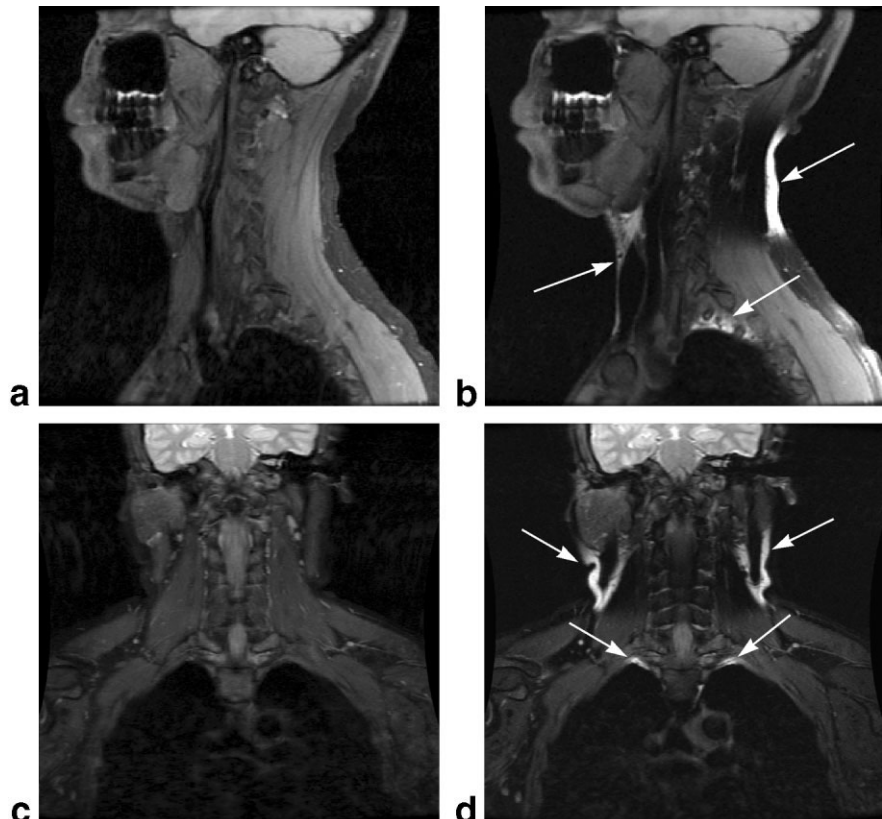
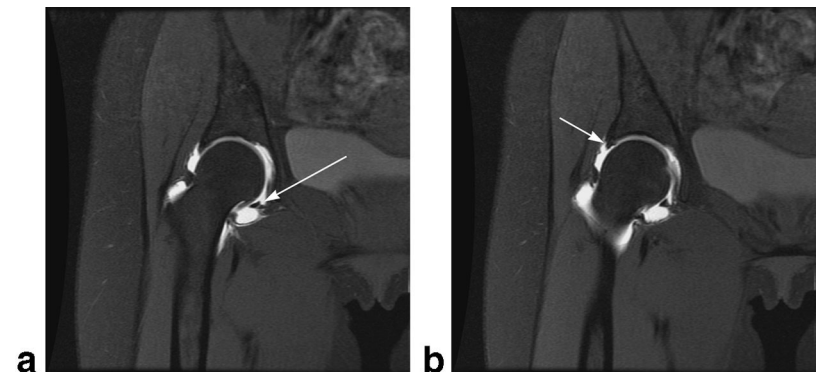


FIG. 10. Coronal T_1 W IDEAL water images from two consecutive slices of an MR hip arthrogram performed after intra-articular injection of dilute Gd-DTPA. Excellent depiction of the transverse ligament (long arrow) and labrum (short arrow) is seen, with uniform suppression of fat across all images. Image parameters: TR/TE = 600/12 ms, matrix = 384×192 , FOV = 20 cm, slice/gap = 4 mm/0.5 mm, ETL = 2, BW = ± 32 kHz, NEX = 2 (“no-phase wrap” on), total scan time for hip = 6 min 30 s.



lines of k -space are acquired first and the outer lines of k -space have substantial T_2 weighting. Blurring should not be problematic for T_2 W and T_1 W imaging because early echoes are weighted to the edges of k -space in T_2 W imaging, and echo trains are short for T_1 W imaging. We have not experienced any subjective increase in blurring with proton-density IDEAL imaging compared to conventional proton-density imaging for typical clinical imaging parameters (ETL = 8–12). The increase in echo spacing will be greater for the IDEAL method than for other FSE water–fat separation methods (7,12,13). For example, the echo spacing for a $(-\pi/6, \pi/2, 7\pi/6)$ combination will increase by 5.5 ms at 1.5T and 2.8 ms at 3.0T. In comparison, the $(0, \pi/2, \pi)$ combination (8,12) will increase the echo spacing by 4.8 ms at 1.5T and 2.4 ms at 3.0T. The latter combination of echoes reduces the increase in echo spacing by only 14%, while the NSA is decreased from 3 to approximately 2 (Fig. 5). For low-bandwidth imaging (± 16 – 32 kHz), the increment in echo spacing required for water–fat separation is a small fraction of the total echo spacing, usually less than 30%. In fact, the overall sequence efficiency of FSE water–fat separation methods may actually improve in comparison with fat-saturation techniques, because the overhead required for the fat-saturation pulse and accompanying crusher gradients is no longer required. This is particularly true for short echo train sequences, especially in T_1 W imaging.

The major disadvantage of most water–fat separation methods is the threefold increase in the minimum scan time. With IDEAL imaging, the SNR efficiency is very high, since all information from source images is used efficiently in the water–fat decomposition. In comparison to a fat-saturated acquisition with three averages, there is no time or SNR penalty. In addition, fat and recombined images are provided in addition to the water image, and are available for review by the radiologist. Finally, while oversampling in the phase-encoding direction, which is commonly used to prevent aliasing (“no phase wrap”), works well with water–fat separation methods, it currently requires an additional doubling of scan time, which is a sixfold increase from the time required for a single source image. Although these acquisitions are also very SNR-efficient, in our experience this increase in scan time is often prohibitive for clinical applications.

Early attempts to reduce the minimum scan time focused on combining parallel imaging (27,28) with water–fat separation methods. Early results have been very prom-

ising (29–31). Parallel imaging plays a complementary role with these methods: increases in acquisition time from water–fat separation methods are offset by parallel imaging, and decreases in SNR from parallel imaging approaches are offset by gains in SNR from water–fat decomposition methods.

Reductions in scan time can also be achieved with partial k -space acquisitions that reduce the number of phase- or depth-encoding steps used (for 3D acquisitions). Partial k -space acquisitions in the readout (frequency) direction are commonly used for ultrashort TR sequences to help reduce TR and first-moment velocity phase shifts from the readout gradient. Such acquisitions depend on homodyne (25) or related reconstruction algorithms (32) to obtain full-resolution images. Unfortunately, these methods de-modulate the phase information from the source images that is needed by water–fat decomposition algorithms to separate water from fat. Zero-filling the k -space matrix is an effective alternative, but reconstructed water and fat images will suffer from blurring in comparison with conventional images reconstructed with partial k -space algorithms (13). Early attempts to apply homodyne reconstruction to water–fat separation methods have been described (12), but this method has only been applied to source images that contain water and fat that are in phase (zero) or out of phase (π), and has not been applied to phase shifts other than zero or π .

A similar analysis of echo optimization can be easily extended to other pulse sequences, including gradient-echo (GRE) and steady-state free precession (SSFP) sequences. For GRE sequences, water and fat are aligned when TE = 0, and all echo shifts are referenced to this time point. Because all echo shifts must be positive, the echo shift for the middle echo of a GRE water–fat separation acquisition that maximizes NSA performance is $\pi/2 + \pi k$ ($k \geq 1$). For example, an optimal echo combination for a three-point GRE acquisition is $(5\pi/6, 3\pi/2, 13\pi/6)$ with corresponding time shifts of 1.98 ms, 3.57 ms, and 5.16 ms at 1.5T, or 0.99 ms, 1.79 ms and 2.58 ms at 3.0T. For SSFP, water, and fat refocus at TE = TR/2 (33,34), and therefore phase shifts for water–fat separation should be referenced to zero at TR/2. At this time point, water and fat will refocus in either an aligned or anti-aligned orientation depending on the TR and the local field inhomogeneity (33,34). The difference between aligned and anti-aligned voxels is equivalent to a π phase shift created by a water–fat chemical shift. Fortunately, a π phase shift will shift one group of optimally spaced echoes to another group

with an identical NSA performance. For example, a SSFP acquisition with phase shifts of $(-\pi/6, -\pi/2, \pi/6)$ with respect to $\text{TE} = \text{TR}/2$, has the same noise performance as effective phase shifts of $(-\pi/6, \pi/2, 7\pi/6)$ or $(-\pi/6, -3\pi/2, -5\pi/6)$, which both have $\text{NSA} = 3$ for all fat:water ratios. Algorithms that optimize echo shifts for SSFP are complex because echo positions affect many sequence parameters that determine TR, while TR determines the reference point ($\text{TR}/2$) of the water–fat phase shifts. A complete discussion of this optimization is beyond the scope of the current study.

CONCLUSIONS

Careful selection of the TE is essential for SE and FSE water–fat separation applications in order to optimize the performance of water–fat decomposition in voxels with varying relative quantities of water and fat. Poor selection of echo shifts may cause image artifacts in calculated water and fat images resulting from variation in the maximum theoretical noise performance for different fat:water ratios within a voxel. Noise performance can be maximized, and its dependence on the fat:water ratio can be eliminated using the IDEAL method. The middle image is acquired with a water–fat phase shift of $\pi/2 + \pi k$ (k = any integer), and the other two images are acquired with phase $-2\pi/3$ and $2\pi/3$ with respect to the middle image. For FSE and SE applications, a practical combination of echo shifts is $(-\pi/6, \pi/2, 7\pi/6)$ or $(-\pi/6, -\pi/2, \pi/6)$ with respect to the center of the SE. In addition, the noise performance of the iterative least-squares water–fat estimation method used in this work matches the theoretical maximum, demonstrating that it is an efficient estimation method. IDEAL separation of fat and water in clinical imaging should have wide applications, including T_2W , T_1W , and proton density imaging with and without intravenous or intra-articular contrast.

ACKNOWLEDGMENT

The authors thank Jane W. Johnson, RT, for her assistance.

REFERENCES

- Bydder GM, Pennock JM, Steiner RE, Khenia S, Payne JA, Young IR. The short TI inversion recovery sequence—an approach to MR imaging of the abdomen. *Magn Reson Imaging* 1985;3:251–254.
- Meyer CH, Pauly JM, Macovski A, Nishimura DG. Simultaneous spatial and spectral selective excitation. *Magn Reson Med* 1990;15:287–304.
- Block W, Pauly J, Kerr A, Nishimura D. Consistent fat suppression with compensated spectral-spatial pulses. *Magn Reson Med* 1997;38:198–206.
- Dixon W. Simple proton spectroscopic imaging. *Radiology* 1984;153:189–194.
- Glover G. Multipoint Dixon technique for water and fat proton and susceptibility imaging. *J Magn Reson Imaging* 1991;1:521–530.
- Glover GH, Schneider E. Three-point Dixon technique for true water/fat decomposition with B_0 inhomogeneity correction. *Magn Reson Med* 1991;18:371–383.
- Hardy PA, Hinks RS, Tkach JA. Separation of fat and water in fast spin-echo MR imaging with the three-point Dixon technique. *J Magn Reson Imaging* 1995;5:181–185.
- Xiang Q, An L. Water–fat imaging with direct phase encoding. *J Magn Reson Imaging* 1997;7:1002–1015.
- An L, Xiang QS. Chemical shift imaging with spectrum modeling. *Magn Reson Med* 2001;46:126–130.
- Rybicki FJ, Chung T, Reid J, Jaramillo D, Mulkern RV, Ma J. Fast three-point Dixon MR imaging using low-resolution images for phase correction: a comparison with chemical shift selective fat suppression for pediatric musculoskeletal imaging. *AJR Am J Roentgenol* 2001;177:1019–1023.
- Rybicki FJ, Mulkern RV, Robertson RL, Robson CD, Chung T, Ma J. Fast three-point Dixon MR imaging of the retrobulbar space with low-resolution images for phase correction: comparison with fast spin-echo inversion recovery imaging. *AJR Am J Neuroradiol* 2001;22:1798–1802.
- Ma J, Singh SK, Kumar AJ, Leeds NE, Broemeling LD. Method for efficient fast spin echo Dixon imaging. *Magn Reson Med* 2002;48:1021–1027.
- Reeder SB, Wen Z, Yu H, Pineda AR, Gold GE, Markl M, Pelc NJ. Multicoil Dixon chemical species separation with an iterative least-squares estimation method. *Magn Reson Med* 2004;51:35–45.
- Wen Z, Reeder SB, Pineda AR, Glover GH, Pelc NJ. Noise performance study of symmetric three point Dixon method. In: Proceedings of the 11th Annual Meeting of ISMRM, Toronto, Canada, 2003. p 483.
- Pineda AR, Wen Z, Reeder SB, Yu H, Pelc NJ. Cramér-Rao bounds for 3-point Dixon imaging. In: Proceedings of the 12th Annual Meeting of ISMRM, Kyoto, Japan, 2004. p 2107.
- Pineda AR, Reeder SB, Wen Z, Yu H, Pelc NJ. Cramér-Rao bounds for 3-point decomposition of water and fat. *Magn Reson Med* 2005;54:625–635.
- Yu H, Reeder SB, Shimakawa A, Brittain JH, Pelc NJ. Robust field map estimation in a Dixon water–fat separation algorithm with short echo time increments. In: Proceedings of the 12th Annual Meeting of ISMRM, Kyoto, Japan, 2004. p 345.
- Reeder SB, Pelc NJ, Alley MT, Gold GE. Rapid MR imaging of articular cartilage with steady-state free precession and multipoint fat–water separation. *AJR Am J Roentgenol* 2003;180:357–362.
- Ma J. Breath-hold water and fat imaging using a dual-echo two-point Dixon technique with an efficient and robust phase-correction algorithm. *Magn Reson Med* 2004;52:415–419.
- Brix G, Heiland S, Bellemann M, Koch T, Lorenz W. MR imaging of fat-containing tissues: valuation of two quantitative imaging techniques in comparison with localized proton spectroscopy. *Magn Reson Imaging* 1993;11:977–991.
- Kay S. In: Oppenheim A, editor. *Fundamentals of statistical signal processing: estimation theory*. Upper Saddle River, NJ: Prentice Hall; 1993. p 83–86.
- Saadeh S, Younossi ZM, Remer EM, Gramlich T, Ong JP, Hurley M, Mullen KD, Cooper JN, Sheridan MJ. The utility of radiological imaging in nonalcoholic fatty liver disease. *Gastroenterology* 2002;123:745–750.
- Mayo-Smith WW, Boland GW, Noto RB, Lee MJ. State-of-the-art adrenal imaging. *Radiographics* 2001;21:995–1012.
- Yamamoto E, Kohno H. Resolution of NMR chemical shift images into real and imaginary components. *Phys Med Biol* 1986;31:713–720.
- Noll DC, Nishimura DG, Macovski A. Homodyne detection in magnetic resonance imaging. *IEEE Trans Med Imaging* 1991;10:154–163.
- Farzaneh F, Riederer SJ, Pelc NJ. Analysis of T_2 limitations and off-resonance effects on spatial resolution and artifacts in echo-planar imaging. *Magn Reson Med* 1990;14:123–139.
- Sodickson DK, Manning WJ. Simultaneous acquisition of spatial harmonics (SMASH): fast imaging with radiofrequency coil arrays. *Magn Reson Med* 1997;38:591–603.
- Pruessmann KP, Weiger M, Scheidegger MB, Boesiger P. SENSE: sensitivity encoding for fast MRI. *Magn Reson Med* 1999;42:952–962.
- Ma J, Banksom J, Stafford R. Multipoint Dixon imaging using sensitivity encoding. In: Proceedings of the 11th Annual Meeting of ISMRM, Toronto, Canada, 2003. p 1069.
- McKenzie CA, Reeder SB, Shimakawa A, Pelc NJ, Brittain JH. Abdominal three point Dixon imaging with self calibrating parallel MRI. In: Proceedings of the 12th Annual Meeting of ISMRM, Kyoto, Japan, 2004. p 917.
- Reeder SB, McKenzie CA, Markl M, Yu H, Pelc NJ, Brittain JH. Parallel cardiac CINE imaging: application to “Dixon” water–fat separation and steady-state free precession. In: Proceedings of the 12th Annual Meeting of ISMRM, Kyoto, Japan, 2004. p 267.
- McGibney G, Smith MR, Nichols ST, Crawley A. Quantitative evaluation of several partial Fourier reconstruction algorithms used in MRI. *Magn Reson Med* 1993;30:51–59.
- Scheffler K, Hennig J. Is TrueFISP a gradient-echo or a spin-echo sequence? *Magn Reson Med* 2003;49:395–397.
- Hargreaves BA, Vasanawala SS, Nayak KS, Hu BS, Nishimura DG. Fat-suppressed steady-state free precession imaging using phase detection. *Magn Reson Med* 2003;50:210–213.